Experimental Investigation of FRP-Strengthened RC Beam-Column Joints

Costas P. Antonopoulos[1] and Thanasis C. Triantafillou, M.ASCE[2]

Abstract: The results of a comprehensive experimental program, aimed at providing a fundamental understanding of the behavior of shear-critical exterior reinforced concrete (RC) joints strengthened with fiber reinforced polymers (FRP) under simulated seismic load, are presented in this study. The role of various parameters on the effectiveness of FRP is examined through 2/3-scale testing of 18 exterior RC joints. Conclusions are drawn on the basis of certain load versus imposed displacement response characteristics, comprising the strength (maximum lateral load), the stiffness, and the cumulative energy dissipation capacity. The results demonstrate the important role of mechanical anchorages in limiting premature debonding, and they provide important information on the role of various parameters, including: area fraction of FRP; distribution of FRP between the beam and the column; column axial load; internal joint (steel) reinforcement; initial damage; carbon versus glass fibers; sheets versus strips; and effect of transverse beams.

Introduction and Background

Recent earthquakes worldwide have illustrated the vulnerability of existing reinforced concrete (RC) beam-column joints to seismic loading. Poorly detailed joints, especially exterior ones, have been identified as critical structural elements, which appear to fail prematurely, thus performing as "weak links" in RC frames. A typical failure mode in poorly designed joints (lacking adequate transverse reinforcement) is concrete shear in the form of diagonal tension. Bond failure of rebars has been observed too, especially in interior joints where rebars are not properly anchored with standard hooks (Paulay and Priestley 1992).

Strengthening of RC joints is a challenging task that poses major practical difficulties. A variety of techniques applicable to concrete elements have also been applied to joints with the most common ones being the construction of RC or steel jackets (Alcocer and Jirsa 1993). Reinforced concrete jackets and some forms of steel jackets, namely steel "cages," require intensive labor and artful detailing. Moreover, concrete jackets increase the dimensions and weight of structural elements. Plain or corrugated steel plates have also been tried (Beres et al. 1992; Ghobarah et al. 1997). In addition to corrosion protection, these elements require special attachment through the use of either epoxy adhesives combined with bolts or special grouting.

More than a decade ago, a new technique for strengthening structural elements emerged. The technique involves the use of fiber reinforced polymers (FRP) as externally bonded reinforcement (EBR) in critical regions of RC elements. FRP materials, which are available today in the form of strips or in situ resin impregnated sheets, are being used to strengthen a variety of RC elements, including beams, slabs, columns, and shear walls, to enhance the flexural, shear, and axial (through confinement) capacity of such elements.
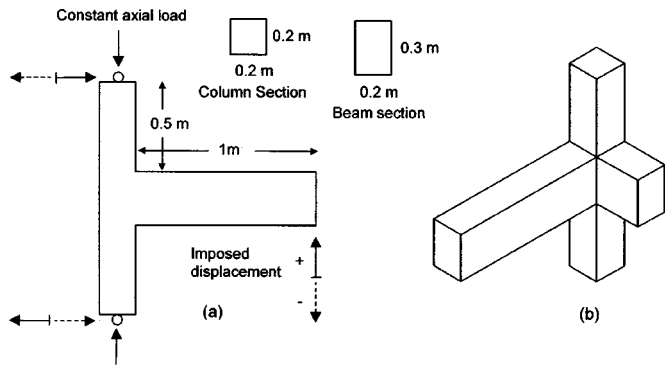
FRP materials have a number of favorable characteristics, including; ease of installation; immunity to corrosion; extremely high strength; availability in convenient "to apply" forms, etc. The authors started a comprehensive research program about 5 years ago that was aimed at expanding the range of applicability of the FRP strengthening technique to poorly detailed shear-critical RC joints. The simplest way to strengthen such joints is to attach (through epoxy bonding) FRP sheets or strips to the joint region with the fibers in two orthogonal directions, those of the beams and columns meeting at the joint. This concept combines ease of application with effectiveness, as the 2D fiber system in the joint will act as shear reinforcement.

FRP-strengthened RC joints have been studied by other investigators, too. Pantelides et al. (1997, 1999) applied quasistatic lateral load tests of two full-scale RC bridge bents strengthened with carbon sheets in the cap beam-column joints; they concluded that the composite wrap increased the shear capacity of the joints by 35%. Gergely et al. (1998) analyzed one of the aforementioned bents by performing pushover analysis and found good agreement between the experimental and theoretical load versus displacement response. Geng et al. (1998) and Mosallam (1999) used composite overlays to strengthen simple models of interior beam-column joints and recorded increases in the strength, the stiffness, and the ductility of the specimens. However, these specimens were not representative of true shear-critical joint behavior, but they behaved more like column-type elements (without axial force) subjected to bending. Yet, strengthening was not applied in the joint itself but in the column ends. Castellani et al. (1999) performed full-scale seismic testing of a 2/3-scale two-story, two-bay RC building at the European Laboratory for Structural Assessment (Ispra). In this building, which was damaged (cracking and slippage of beam rebars), repaired, strengthened with carbon

[1]Graduate Research Assistant, Dept. of Civil Engineering, Univ. of Patras, Patras 26500, Greece.

[2]Associate Professor, Dept. of Civil Engineering, Univ. of Patras, Patras 26500, Greece. E-mail: ttriant@upatras.gr

Fig. 1. (a) Geometry of specimens; (b) transverse beam (joints T-C, T-F33, T-F22S2)

Fig. 2. Details of reinforcement

fiber reinforced polymer (CFRP) in the joints, and retested, composite materials proved to be good candidates for strengthening of joints if the proper detailing was implemented. Tsonos and Stylianidis (1999) performed one simulated seismic load test of an exterior joint model strengthened with FRP. He recorded considerable increase in the strength, the energy dissipation and the stiffness characteristics compared to the control (unstrengthened) specimen. Finally, Gergely et al. (2000) tested a series of 1/3-scale exterior beam-column joints strengthened with carbon sheets. Main variables in this investigation were the concrete surface preparation and the fiber orientation, and the main conclusion was that FRP composites provide a viable solution in improving the shear capacity of exterior RC joints.
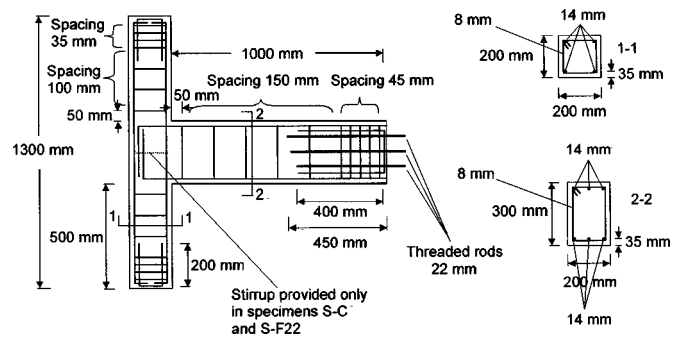
In this study, the authors present the results of a comprehensive experimental program, which was aimed at providing a fundamental understanding of the behavior of shear-critical exterior RC joints strengthened with composite materials under simulated seismic load, through the investigation of a number of design parameters. We believe that the present study presents an advancement of the state-of-the-art in this area, as it deals systematically with the effect of several design variables for the first time. Details are provided next.

Experimental Program

Description of Test Specimens

A total of 18, 2/3-scale, reinforced concrete joints were constructed and tested, as shown in Fig. 1(a). All the specimens had identical dimensions and were reinforced such that they would represent a poorly detailed exterior T joint of a RC frame. Reinforcement consisted of four, 14-mm diameter rebars in the column, three 14-mm diameter rebars in each side (top, bottom) of the beam, 8-mm stirrups at a spacing of 10 mm in the column, and 8-mm stirrups at a spacing of 15 mm in the beam. Sixteen of the specimens had no stirrups in the joint, and the remaining two specimens had only one column stirrup in the joint. Details of the reinforcement are shown in Fig. 2. Three of the 16 specimens (without stirrup in the joint) were not planar, but they were constructed with a transverse beam in one side [Fig. 1(b)] to account for the effect of confinement provided by transverse elements. Reinforcement in the transverse beams consisted of four, 14-mm diameter longitudinal rebars.

A crucial point to emphasize is that *all* specimens were designed such that failure would be due to shear in the joint. This

was an important requirement, as one of the main objectives in this study was to evaluate the contribution of FRP to the *shear capacity* of RC joints. Moreover, the specimens were designed such that the effect of a series of factors on the shear capacity of joints could be investigated. These factors included the following: effectiveness of strips versus sheets; number of strips or number of sheet layers; mechanical anchorages; type of fibers (carbon versus glass); level of axial load in the column; damage in the joint prior to strengthening; and effect of transverse beam. The design was assisted by an analytical model developed by the authors based on fundamental mechanics (stress equilibrium and strain compatibility) of the joint core (Antonopoulos and Triantafillou 2002). The designs of all the tested joints and details of the alternative strengthening configurations examined are given in Fig. 3. A short description of the specimens follows.

- C1 and C2 were used as control specimens (without FRP); their only difference was in the strength of concrete, which was equal to 19.4 MPa for C1 and 23.7 MPa for C2.
- S33 had three carbon strips on each side of the beam and three on each side of the column.
- S63 had six carbon strips on each side of the beam and three on each side of the column.
- S33L was identical to S33 with L-shaped mechanical anchors provided in the ends of the beam. These anchors consisted of a pair of 5-mm thick and 300-mm long unequal leg steel angles, with legs equal to 35 mm and 60 mm. The two angles were bonded to the two edges of the column with epoxy adhesive and connected with each other through a transverse welded steel plate (Fig. 3). Note that such anchors do not have to (and should not) be made of steel, but they were made as such in this study for simplicity.
- F11 had one layer of flexible sheet (made of carbon fibers) on each side of the column and one layer of U-shaped sheet on the beam.
- F22 was identical to F11 but with two layers of sheets on both the beam and the column.
- F21 had two layers of sheet on the beam and one on each side of the column.
- F12 had one layer of sheet on the beam and two on each side of the column.
- F22A was identical to F22, but this was the only specimen where the axial force in the column was different (115 kN) from all the others (46 kN).
- F22W was identical to F22 but with improved anchorage of the sheets in a short distance outside the joint. This anchorage was provided by wrapping two layers of 150-mm wide sheets at the ends of the three members (two columns, one beam) meeting at the joint.
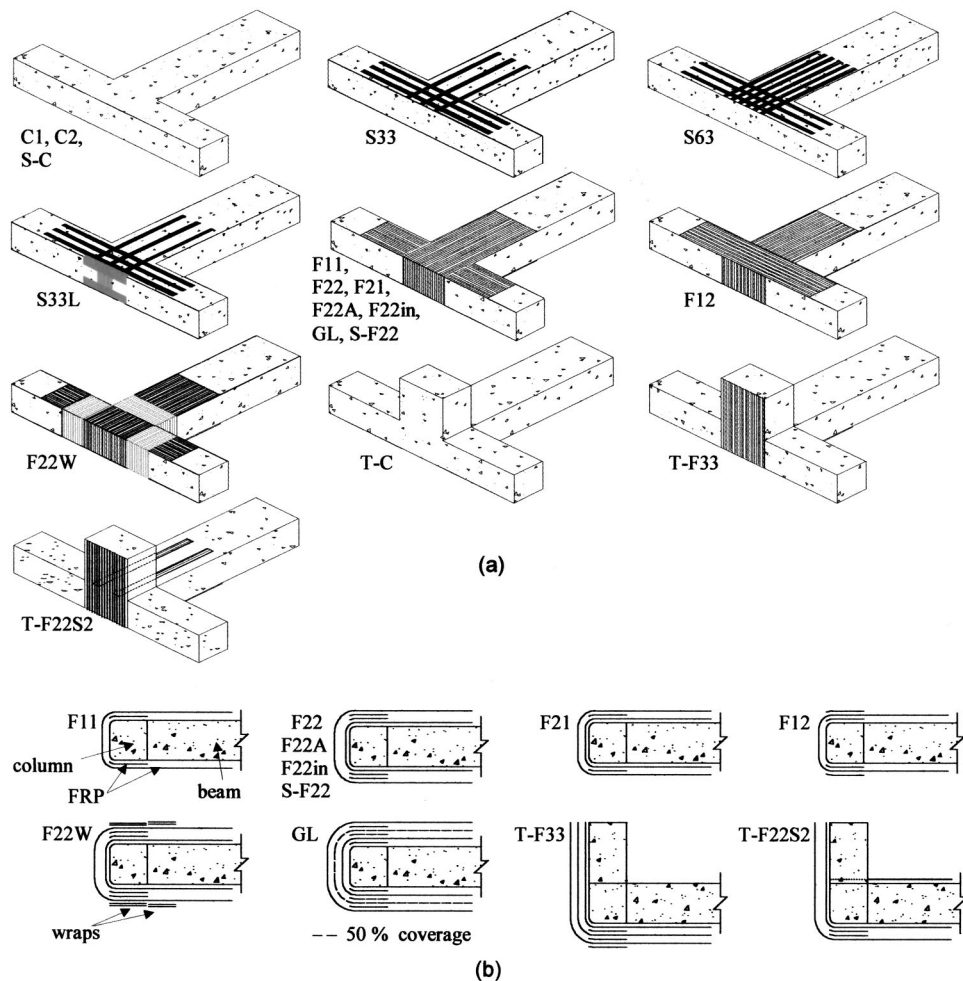
Fig. 3. (a) Description of specimens and strengthening alternatives; (b) layout of FRP layers

- F22in was identical to F22 but strengthened after a certain degree of initial damage had occurred in the virgin specimen. The damage was induced by preloading the specimen at an imposed displacement, which reached a maximum level of 10 mm. Then the specimen was unloaded and application of the FRP took place.
- GL was the only specimen strengthened with glass fibers. It had 2-1/2 (to be explained below) of glass fiber sheet on each side of the column and on the beam (in a U-shaped configuration).
- S-C was a control specimen with one stirrup in the joint.
- S-F22 was identical to F22 but contained one stirrup in the joint.
- T-C was used as control specimen with one transverse beam.
- T-F33 had three layers of sheet on the side of the column opposite to the transverse beam and another three layers of an L-shaped jacket covering the free side of the main beam as well as that of the transverse beam.
- T-F22S2 was identical to T-F33 but with two instead of three layers of sheets. In addition, it had two strips on the interior side of the beam (with total cross sectional area equal to the area of the three strips used for specimens S33 and S33L). In the joint region, the strips were inserted in holes, which were drilled through the thickness of the transverse beam.

The FRP strips used to strengthen specimens S33, S63, and S33L were 25-mm wide and 1.05-mm thick, and those for specimen T-F22S2 were 37.5-mm wide and 1.05-mm thick. The nominal thickness of sheets was 0.13 mm and 0.17 mm for carbon and glass, respectively. The resulting area fractions of FRP reinforcement (defined as the cross-sectional area of FRP divided by the member's cross-sectional area) in the beam and the column, ρ_{fb} and ρ_{fc}, respectively, are given in Table 1.

Finally, in all cases the FRP covered the joint region and extended 450 mm and 300 mm in the beam and the column, respectively.

Preparation of Specimens

The concrete was prepared using type II portland cement (containing about 20% by weight of pozzolans) and crushed aggregates with a maximum size of 15 mm in a water:cement:aggregate ratio of approximately 0.65:1:6.4 by weight. Casting of the specimens took place in T-shaped steel molds, which were placed horizontally. The specimens were cured using wet burlaps for 1 week and then left in room conditions. Bonding of the composite materials took place at a concrete age of about 30–35 days. To ensure a high quality bond between the concrete and the FRP reinforcement, the specimens were thoroughly wire brushed (sur-

Table 1. Specimen Data and Results

| Specimen | 28 Day Concrete Strength (MPa) | FRP Area Fraction | | Maximum Load | | Percent Difference with Control | |
		Beam ρ_{fb} (%)	Column ρ_{fc} (%)	Push (kN)	Pull (kN)	Push	Pull
C1	19.5	0	0	31.32	27.13		
C2	23.7	0	0	30.82	31.08		
Average C1,C2	21.6	0	0	**31.07**	**29.10**	**0**	**0**
S33	26.0	0.26	0.39	34.66	35.28	11.6	21.2
S63	24.2	0.52	0.39	39.36	40.24	26.7	38.3
S33L	26.3	0.26	0.39	44.63	40.40	43.6	38.8
F11	22.8	0.13	0.13	42.76	42.44	37.6	45.8
F22	27.2	0.26	0.26	50.04	49.14	61.0	68.1
F21	27.0	0.26	0.13	51.08	50.29	64.4	72.8
F12	29.5	0.13	0.26	44.45	44.40	43.1	52.6
F22A	27.8	0.26	0.26	57.38	52.56	84.7	80.6
F22W	29.2	0.26	0.26	55.84	54.89	79.7	88.6
F22in	21.0	0.26	0.26	41.93	41.59	35.0	42.9
GL	19.5	0.42	0.42	44.13	43.04	42.0	47.9
S-C	19.3	0	0	**33.27**	**32.22**	**0**	**0**
S-F22	19.0	0.26	0.26	44.09	43.23	32.5	34.2
T-C	24.6	0	0	**36.02**	**33.86**	**0**	**0**
T-F33	26.0	0.19	0.19	44.26	44.45	22.9	31.3
T-F22S2	22.0	0.26	0.13	40.07	39.75	11.2	17.4

faces which received strips were roughened using a small hammer), until any loose material was removed and vacuumed. In those specimens where the external reinforcement had to turn around sharp edges (column edges), grinding of the concrete was provided to a radius of about 25–30 mm.

The outline of the external reinforcement layout was marked on the specimens, and the FRP was cut to the required length. The FRP materials used were of two types: pultruded carbon strips; and flexible carbon or glass sheets. The strips were cleaned with acetone and bonded through the use of a two-part epoxy adhesive. Proper bonding and removal of excessive adhesive was achieved using a plastic roller. Bonding of the sheets took place in several steps, which included: application of a two-part epoxy adhesive on the concrete; bonding of the first FRP layer; application of epoxy and impregnation of the sheet using a plastic roller; application of the next layer of sheet; etc.

To take advantage of the ability provided by the sheets to turn around the column (thus ensuring a good anchorage of the FRP reinforcement in the vicinity of the two column edges), in most specimens, the last FRP layer was always applied on the beam. Details of the application sequence of the various layers are given in Fig. 3(b).

Specimen GL deserves special mention. The number of layers for this specimen was determined such that the FRP jacket would have the same axial rigidity as that for specimen F11 (with one layer in the column and one in the beam). The ratio of the products (thickness of sheet×elastic modulus) for carbon and glass sheets was calculated approximately equal to 2.5, meaning that the equivalent of one layer of carbon sheet would be "two and a half" layers of glass sheet. The "half" layer was achieved by cutting the sheet in narrow strips and using them to construct the second layer of the jacket (in both the beam and the column) with partial (50%) coverage of the beam and column sides. Three 33-mm wide strips were used for the column at a 63-mm spacing, and three 50-mm wide strips were used for the beam at a 95-mm spacing.

As described above, two of the specimens, S33L and F22W, had special anchorage devices. In S33L, the anchorage of the

strips near the column edges was improved by using steel angles. These angles were epoxy-bonded against the two column edges, providing a 35-mm overlap at one end of the strips. To provide for a flat surface on the exterior column sides, the gap between the three strips and the concrete was filled with epoxy so that the thickness of the epoxy layer between the steel angle and the concrete (on the faces of the specimen) exceeded that of the epoxy layer between the steel angle and the strips by an amount equal to the strip thickness.

Finally, an interesting feature was introduced in specimen T-F22S2. In addition to the sheets, this joint received two strips in the interior side of the beam. The strips were inserted into about 45-mm maximum diameter elliptical holes, which were first drilled and then wire brushed and thoroughly cleaned. Following placement of the strips, the holes were filled with epoxy mortar through injection. An interesting feature of the strips used for this joint was the preparation of their ends to maximize their anchoring capacity inside the holes. These ends were first covered by an epoxy adhesive layer of varying thickness and then sand-coated (before hardening of the adhesive), to increase interlock with the surrounding epoxy mortar.

Material Properties

The compressive strength of concrete for each specimen was determined from four, 150-mm cubes taken during casting of each joint. The results for the 28-day average compressive strength are given in Table 1. The steel used for longitudinal reinforcement was type S500 with average yield stress, determined from three specimens equal to 585 MPa. Stirrups were made of mild steel type S220 with average yield stress equal to 260 MPa.

The following properties (average values) were provided by the manufactures for the composite materials: elastic modulus and failure strain of carbon strips=150 GPa and 0.016, respectively; elastic modulus and failure strain of carbon sheets=230 GPa and 0.015, respectively; elastic modulus and failure strain of glass sheets=70 GPa and 0.031, respectively.
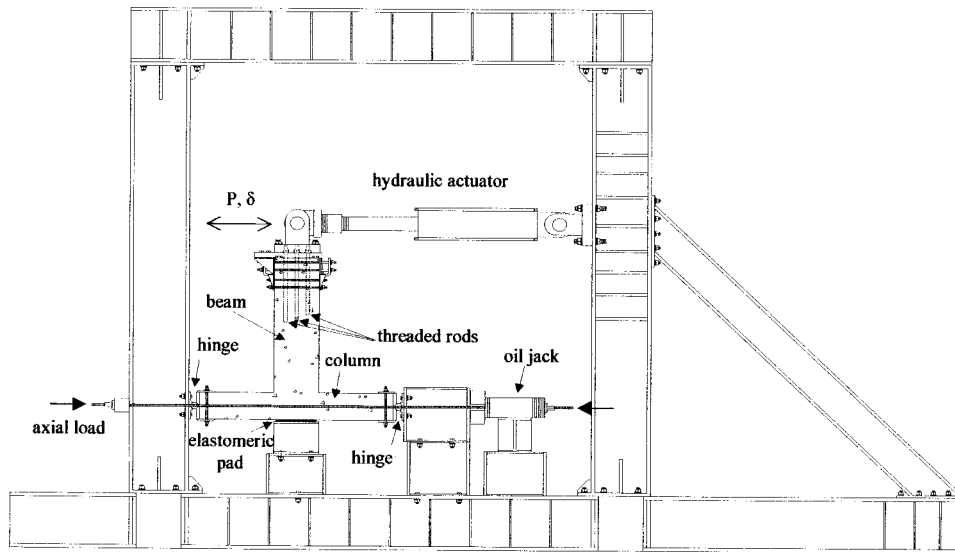
Fig. 4. Schematic view of test setup

Experimental Setup and Procedure

The joints were rotated 90° from their characteristic position in a typical RC frame and were mounted on a stiff steel frame as shown schematically in Fig. 4. In this configuration, the column longitudinal axis was horizontal, and the beam longitudinal axis was vertical. Testing of each model began by slowly applying loads to simulate axial loading of the column. This was accomplished by stressing two high-strength steel rods placed outside the column through the use of a hydraulic load jack. During testing, application of the axial load was controlled manually and kept constant at a level of 46 kN for all specimens except for F22A, which received a force of 115 kN.

Once the full axial load had been applied, earthquake lateral loads were simulated by applying an alternating force to the end of the beam through an idealized pin. This force was applied in a quasistatic cyclic pattern using a horizontally positioned 500 kN MTS actuator. Data from the load cell and the actuator's displacement transducer were recorded using a computer controlled data acquisition system.

An important point during testing was the transfer of the force from the actuator to the beam. This was achieved through a combination of a metallic cap, which confined the beam's free end, and a set of three, 22-mm diameter threaded rods, which were attached inside the moulds before casting; the free ends of these rods were bolted tight on the metallic cap plate (Fig. 4). It is believed that this combination of confining cap and built-in rods provided an effective and slip-free attachment of the actuator to the beam.

The displacement-controlled loading sequence for each specimen consisted of three cycles at a series of progressively increasing (by 5 mm) displacement amplitudes in each direction (push and pull). The loading history is illustrated in Fig. 5.

Experimental Results

Behavior

The response of all joints tested (except for S33) is given in Fig. 6. The hysteresis loops obtained are characterized by substantial pinching, which is typical of joint shear failure. This failure mechanism developed in the form of diagonal cracking in the joint and was observed in all tests (for other than the control specimens where the concrete surface was not visible; the FRP had to be removed in order to allow for visual inspections). Hence, the key objective of strengthening the joints while maintaining the shear failure mode was achieved. A typical diagonal cracking pattern corresponding to shear failure is illustrated in Fig. 7(a).

Note that certain parts of the hysteresis loops obtained for specimen S33 were not considered reliable due to friction and slip problems between the specimen and the supports. Hence, these loops were not considered correct and are not presented in Fig. 6.

In the *control* specimens (C1 and C2 without stirrup in the joint, S-C with one stirrup in the joint, and T-C with transverse beam and no stirrup in the joint) diagonal cracking appeared at a displacement between 10–15 mm.

Specimens with Strips

In specimens S33 and S63, gradual debonding of the beam strips from the face of the beam was observed, initiating at the ends of the strips in the joint region [Fig. 7(b)], when the displacement was about 15–20 mm (near 20 mm for S33 and near 15 mm for S63). Debonding of the beam strips in the joint caused debonding initiation of the column strips, too, especially of the outermost one, in the region around their midlength, due to uplift forces. As the displacement increased and the debonded areas of beam and
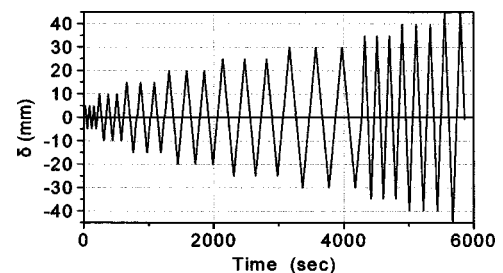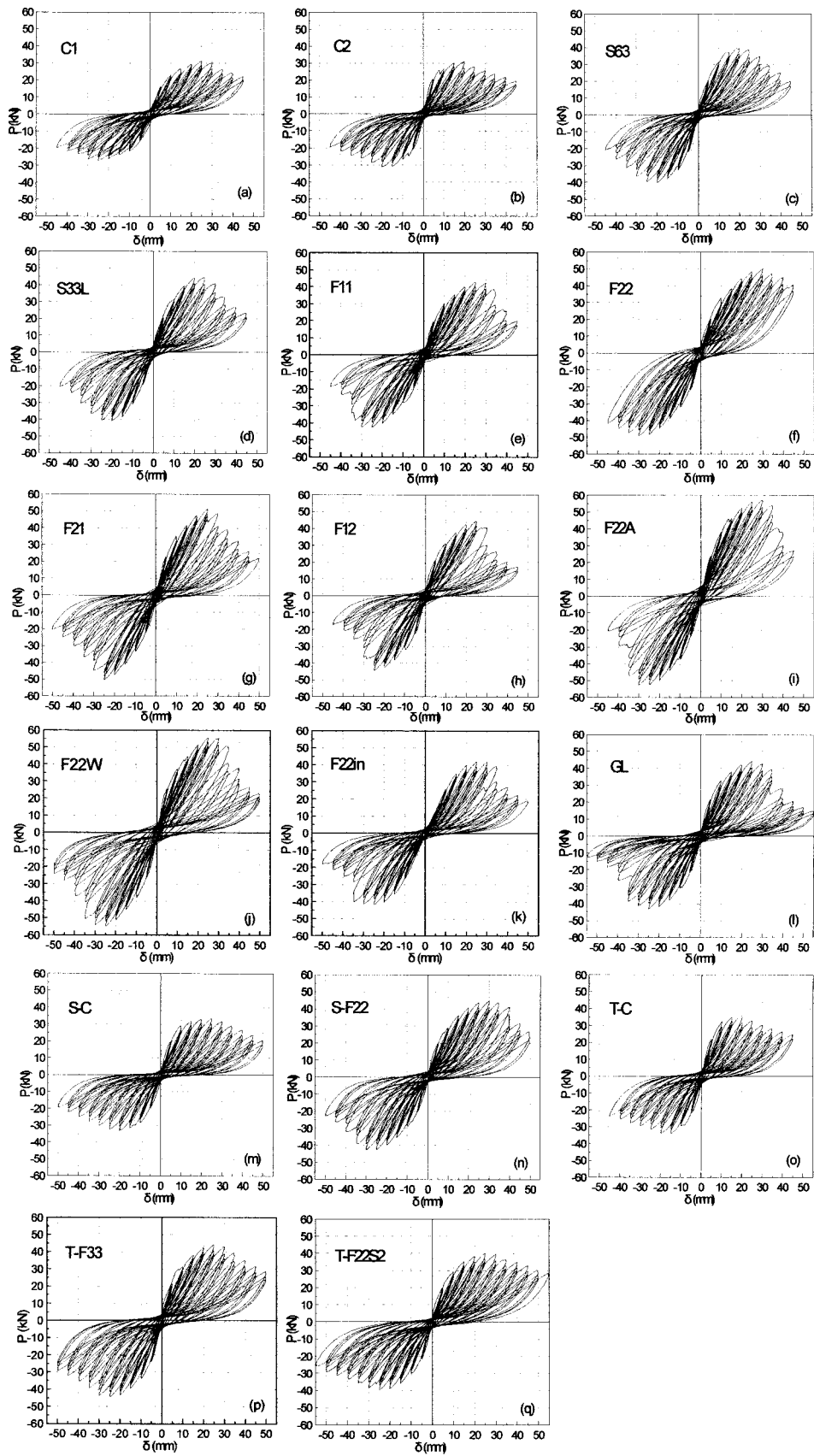

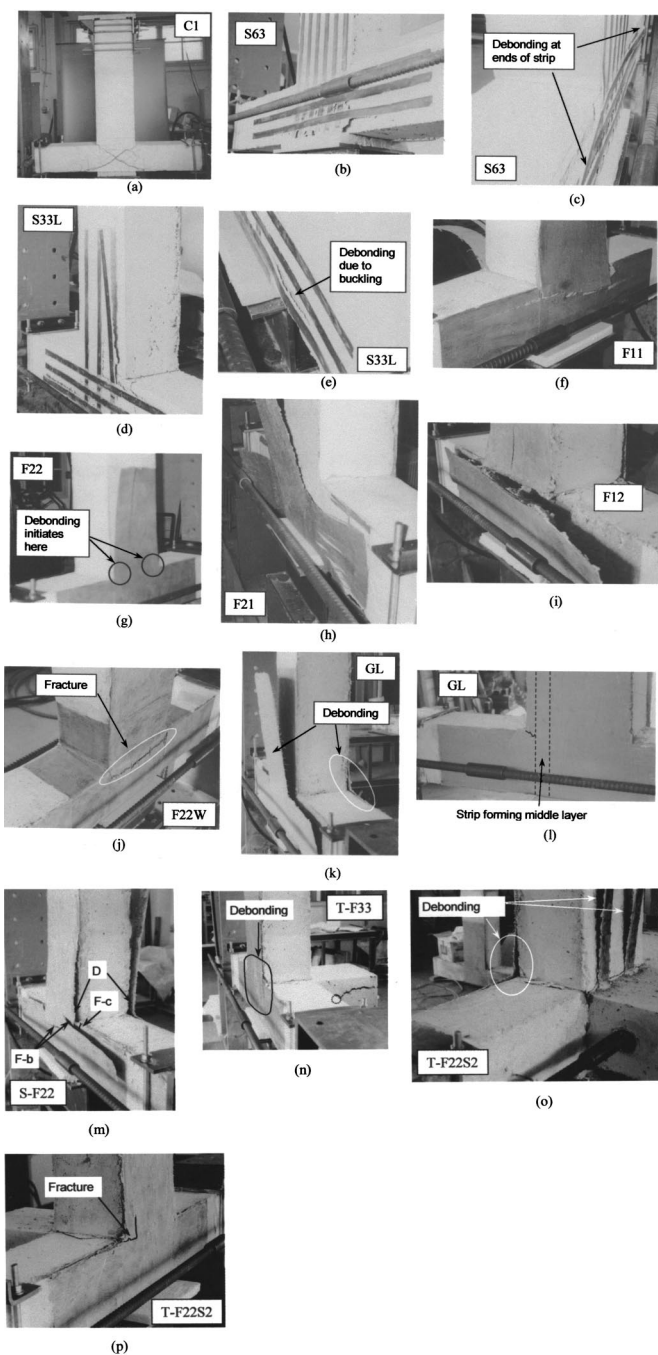**Fig. 5.** Displacement history

Fig. 6. Load versus displacement curves

Fig. 7. Typical photographs of specimens tested

started near the corners of the joint at a displacement of 20 mm. On one side of the beam, debonding propagated gradually towards the end of the sheet [back of specimen in Fig. 7(f)]. Full debonding was observed at a displacement of about 40 mm; whereas on the other side [front of specimen in Fig. 7(f)] debonding was followed by tensile fracture of the beam FRP. This fracture occurred through a horizontal crack, which propagated gradually until the entire beam FRP fractured perpendicular to the fibers (at a displacement of 35 mm), causing partial fracture of the column FRP due to tension perpendicular to the fibers [Fig. 7(f)].

In specimen F22 (with two layers of carbon sheets on each side of the column), fracture of the sheet did not occur but debonding developed similarly to F11; debonded areas developed near the corners until a fraction of the beam FRP was detached and debonded all the way to the free end [Fig. 7(g)]. Specimen F21 (with two layers of sheets on each side of the beam and one on each side of the column) was characterized by full debonding of both the beam and the column FRP on one side [Fig. 7(h)], and by limited debonding near the corners, combined with limited tensile fracture of the column FRP (near the corners) on the other side. The main characteristic of the response of specimen F12 (with one layer of FRP on each side of the beam and two on each side of the column) was full tensile fracture [Fig. 7(i)] of the beam FRP on one side (this followed debonding in the region underneath the fracture line) and full debonding (which developed gradually though) of the sheets on the other.

Specimen F22A (identical to F22 but with higher axial load in the column) developed similar failure characteristics to specimen F11 (fracture of the beam FRP on one side and partial debonding of the beam FRP on the other). In specimen F22W, which had special FRP wrappings at the beam and column ends, debonding was extremely limited. The beam FRP started fracturing on both sides at a displacement of about 20 mm. Cracks in the sheets propagated in a stable manner as the displacement increased until full fracture of the beam layers on one side occurred at a displacement of 35 mm [Fig. 7(j)]. Full fracture of the layers on the opposite side was completed when the displacement reached 40 mm.

Specimen F22in was loaded before strengthening up to a displacement of 10 mm (two series of three cycles each at a 5 mm increment), unloaded, strengthened, and then reloaded. At the end of preloading, diagonal cracking in the joint was already visible (although barely). Upon reloading the strengthened specimen and during the loading history, pinching became more intense as a result of precracking. Failure of the FRP sheet progressed through debonding, similarly to specimen F22, with the following two differences: (1) on one side of the joint, debonding of the FRP was full; and (2) on the other, it was mainly observed in the inner part of the column.

Specimen GL was the only one strengthened with glass fiber sheets. Debonding of the glass fiber reinforced polymer (GFRP) jacket started near the corners (at a displacement of about 20 mm) and propagated until the jacket was fully detached from the joint on one side [Fig. 7(k)]. On the other side of the specimen, where debonding was less severe and rather localized in the vicinity of the joint (near the end of the beam), minor tensile fracture of the beam sheet initiated when the displacement reached 30 mm and propagated slowly until the crack tip reached the part of the sheet which consisted of three layers [Fig. 7(l)].

The next specimen, S-F22, was identical to F22, but had one extra stirrup in the joint. Failure of the FRP occurred according to the following sequence: debonding near the corners (started at a displacement of 15 mm), which spreaded gradually [D in Fig.

column strips increased in a stable manner (in the joint region), the innermost column strips debonded suddenly at their ends due to the high tensile forces transferred [Fig. 7(c)]. Specimen S33L (with the steel angle providing improved anchorage to the beam strips) behaved in a different manner. Debonding initiated in the nonanchored end of a beam strip [Fig. 7(d)] due to tension (at a displacement of 15 mm), but it also developed in column strips—first in compression [Fig. 7(e)] due to local buckling at a displacement of 25 mm and then in tension at a displacement of about 30 mm [Fig. 7(d) bottom left].

Specimens with Sheets (No Stirrup in the Joint, No Transverse Beam)

Specimen F11 was reinforced with one layer of carbon sheet on each side of the beam and the column. Debonding of the sheet

Table 2. Stiffness at Various Displacements and Percent Degradation

Specimen	5 mm	Percent difference	25 mm	Percent difference	Percent degradation	45 mm	Percent difference	Percent degradation
Average C1,C2	3.67	0	1.15	0	68.7	0.45	0	87.7
S33	3.39	−7.6	1.40	21.7	58.7	0.51	13.3	85.0
S63	3.94	7.4	1.56	35.7	60.4	0.46	2.2	88.3
S33L	4.00	9.0	1.70	47.8	57.5	0.48	6.7	88.0
F11	3.92	6.8	1.70	47.8	56.6	0.43	−4.4	89.0
F22	4.24	15.5	1.93	67.8	54.5	0.92	104.4	78.3
F21	4.50	22.6	2.03	76.5	54.9	0.57	26.7	87.3
F12	4.37	19.1	1.78	54.8	59.3	0.38	−15.5	91.3
F22A	4.80	30.8	2.18	89.6	54.6	0.53	17.8	89.0
F22W	5.16	40.6	2.22	93.0	57.0	0.61	35.5	88.2
F22in	2.63	−28.3	1.67	45.2	36.5	0.49	8.9	81.4
GL	4.34	18.3	1.74	51.3	59.9	0.44	−2.2	89.9
S-C	3.95	0	1.31	0	66.8	0.51	0	87.1
S-F22	4.00	1.3	1.73	32.1	56.7	0.65	27.5	83.7
T-C	4.37	0	1.29	0	70.5	0.54	0	87.6
T-F33	4.55	4.1	1.77	37.2	61.1	0.71	31.5	84.4
T-F22S2	4.17	−4.6	1.60	24.0	61.6	0.72	33.3	82.7

7(m)]; initiation of tensile fracture of the column FRP at a displacement of +25 mm [F-c in Fig. 7(m)]; initiation of tensile fracture of the beam FRP at a displacement of −25 mm, and crack propagation until nearly complete fracture at a displacement of +40 mm [F-b in Fig. 7(m)]; nearly complete debonding of the column FRP and part of the beam FRP at end of test.

Specimens with Transverse Beam

FRP failure in specimen T-F33 (with three layers of sheet on the beams and the column) initiated with debonding near the corners at a displacement of 25 mm. When the displacement reached about 30–35 mm, the transverse beam suffered splitting [Fig. 7(n)]; this may be attributed to the lack of stirrups (omitted in the transverse beam) and the presence of a relatively large duct, which was used to accommodate one of the prestressing rods. Until the end of the test, debonding propagated and covered the whole area of the joint panel.

Specimen T-F22S2 had two layers of carbon sheets in the beams (outer side) and the column and two strips in the inner side of the beam, anchored inside the transverse beam at the section where it meets the joint. Failure of the FRP initiated with partial debonding of one strip (in tension) when the displacement reached −20 mm and debonding of the sheets at the corners [Fig. 7(o)]. This was followed by tensile fracturing of the beam FRP near the corners [Fig. 7(p)], with horizontal cracks initiating at displacement of about 20–25 mm. At a displacement level of 35 mm both strips debonded. The test stopped when the displacement reached 55 mm; up to that level the cracks in the sheet progressed slowly.
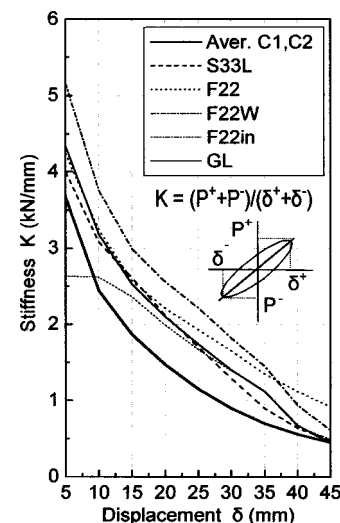
Strength, Stiffness, Energy Dissipation

To evaluate the effectiveness of the various FRP reinforcement configurations, the strength, the stiffness, and the energy dissipation capacity for every load cycle were recorded. The strength (maximum load) in both the push and the pull direction is given in Table 1. The stiffness, which corresponds to the peak-to-peak slope of each first out of three cycles of equal displacement, is provided in Table 2 for various displacement levels. The same table also gives: the stiffness increase with respect to the control

specimen at three displacement levels (5, 25, and 45 mm); and the stiffness degradation at two displacement levels (25 and 45 mm), as a percentage of the stiffness corresponding to the displacement level of 5 mm. Typical stiffness versus imposed displacement curves for various of the joints tested are shown in Fig. 8. Finally, energy dissipation due to inelastic action within and near the joint panel was computed by summing the area enclosed within the load versus displacement curves. The cumulative energy corresponding to the 10, 20, 30, and 40 mm displacement levels is given in Table 3 and in graphical form for some of the specimens tested in Fig. 9.

Analysis of Results

All the joints tested failed as designed, that is in shear, which developed in the form of diagonal cracks in the concrete. In terms of the various factors examined in this investigation, careful ex-

Fig. 8. Typical curves of stiffness versus displacement

Table 3. Energy Dissipation at Various Displacements

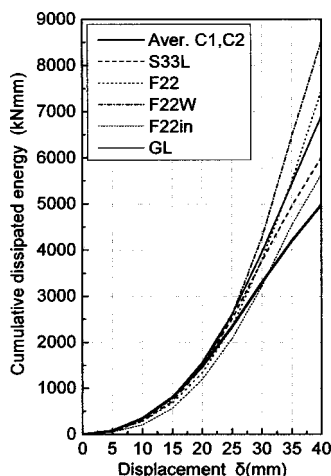| Specimen	Energy Dissipated (kN mm) and Percent Difference with Control Specimen							
	10 mm	Percent difference	20 mm	Percent difference	30 mm	Percent difference	40 mm	Percent difference
Average C1,C2	356	0	1,480	0	3,304	0	4,995	0
S33	—[a]	—[a]	—[a]	—[a]	—[a]	—[a]	—[a]	—[a]
S63	285	−19.9	1,466	−0.9	3,558	7.7	5,763	**15.4**
S33L	300	−15.7	1,473	−0.5	3,775	14.3	6,015	**20.4**
F11	313	−12.1	1,401	−5.3	3,656	10.7	6,395	**28.0**
F22	289	−18.8	1,344	−9.2	3,803	15.1	7,477	**49.7**
F21	323	−9.3	1,490	0.7	4,237	28.2	7,050	**41.1**
F12	321	−9.8	1,415	−4.4	3,961	19.9	6,085	**21.8**
F22A	285	−19.9	1,511	2.1	4,275	29.4	8,417	**68.6**
F22W	333	−6.5	1,486	0.4	4,281	29.6	8,532	**70.8**
F22in	206	−42.1	1,192	−19.5	3,219	−2.6	5,641	**12.9**
GL	343	−3.7	1,565	5.7	3,958	19.8	6,912	**38.4**
S-C	343	0	1,550	0	3,487	0	5,494	**0**
S-F22	320	−6.7	1,393	−10.1	3,532	1.3	6,472	**17.8**
T-C	371	0	1,714	0	3,748	0	5,873	**0**
T-F33	369	−0.5	1,761	2.74	4,451	18.8	7,695	**31.0**
T-F22S2	319	−14.0	1,396	−18.6	3,480	−7.2	6,207	**5.7**

[a]Part of the hysteresis loops for this specimen is not correct, and the energy results are not reliable; hence, they are omitted.

amination of the test results in terms of *strength* (average increase in the push and pull direction) and *energy dissipation* (at the end of the 40 mm cycles) revealed the following information:

- *Increased area fraction in both the beam and the column* (average of C1-C2 versus F11 and F22). Both the strength and the dissipated energy increased considerably with, but not proportionally to, the number of FRP layers. The strength increase is about 40% and 65% for $\rho_{fb}=\rho_{fc}=0.0013$ and 0.0026, respectively; and the associated values for energy dissipation are about 30% and 50%. That is, the two layers acting together have an effectiveness of approximately 65% compared to the action of individual layers: $(65-40)/40 \approx 65\%$, $(50-30)/100 \approx 65\%$.
- *Increased area fraction in the beam only* (average of C1-C2 versus S33 and S63, and versus F11, F21). In terms of strength, increasing the FRP area fraction in the beam is nearly as effective as it is for equal increase in both the beam and the column, implying that the effectiveness of column FRP is rather limited. The strength increase in joints with *strips* is about 15% and 30% for $\rho_{fb}=0.0026$ and 0.0052 (with $\rho_{fc}=0.0039$ in both cases), respectively; the associated energy values are about 15% and 20%. In joints with *sheets*, the strength increase is about 40% and 70% for $\rho_{fb}=0.0013$ and 0.0026 (with $\rho_{fc}=0.0013$ in both cases), respectively; and the associated energy values are about 30% and 40%.

- *Effectiveness of beam versus column FRP reinforcement* (average of C1-C2 versus F21, F12). Beam reinforcement is much more effective than column reinforcement. This may be seen by comparison of results for specimens with $\rho_{fb}=2\rho_{fc}=0.0026$ and $\rho_{fc}=2\rho_{fb}=0.0026$, which indicate a strength increase in the order of 70% and 50%, respectively. The corresponding values for energy dissipation are approximately 40% and 20%.

- *Effect of mechanical anchorage* (F22 versus F22W, S33 versus S33L). The mechanical anchorages employed in this study increased the effectiveness of FRP *sheets* in terms of strength and energy by about 30% (from 65% increase to 85%) and 40% (from 50% increase to 70%), respectively. For *strips*, the effectiveness of anchorage was much higher in the order of 150%—strength increases of about 15% (S33) jumped up to about 40% (S33L).

- *Effect of axial load on strengthened joints* (F22 versus F22A). The favorable effect of high axial load on the shear capacity of FRP-strengthened joints was confirmed. A 2.5 times higher load pushed the strength increase from 65% to about 85% and the energy increase from 50% to 70%.

- *Effect of initial damage* (F22 versus F22in). The initial damage (caused by loading the specimen at 60% of ultimate load) affected adversely the response of the strengthened joint. Strength and energy increases for the undamaged joint were about 65% and 50%, respectively. For the precracked joint, these values dropped to about 40% and 15% indicating that if the strengthened joint is damaged (but not repaired), FRP materials are less effective in terms of energy dissipation as opposed to strength increase.

- *Carbon versus glass FRP* (F11 versus GL). Glass fibers

Fig. 9. Typical curves of energy dissipation versus displacement.

proved only slightly more effective than carbon fibers in terms of strength but more effective in terms of energy dissipation (about 30% energy increase in F11 versus 40% in GL).

- *Sheets versus strips* (S33L versus F22). Joints S33L and F22 had the same FRP area fraction in the beam and different in the column. Despite the higher FRP area fraction in the column (0.0039 versus 0.0026), the specimen with strips performed worse than that with sheets. The increase in strength and energy was 40% and 20%, respectively, in S33L, whereas the corresponding values for F22 reached 65% and 50%. This result is not surprising, as the achievement of proper anchorages for strips is a much more difficult task than for sheets; yet, the sheets provide a more even transfer of forces over the joint region.

- *Effectiveness of FRP versus steel reinforcement (stirrups) in the joint* (average of C1-C2 versus F22 and S-C versus S-F22). As the transverse steel reinforcement in the joint increased, the FRP became less effective. Area fractions $\rho_{fb} = \rho_{fc} = 0.0026$ in the joint without the extra stirrup provided a 65% and 50% increase in the strength and the energy, respectively, whereas the associated values for the joint with one extra stirrup were about 35% and 20%.

- *Effectiveness of FRP on joints with transverse beam* (T-C versus T-F33 and average of C1-C2 versus average of F11-F22; T-C versus T-F22S2 and average of C1-C2 versus F21). For the case of FRP sheets making a 90° turn, the presence of a transverse beam decreased the effectiveness of the FRP by about 50% and 20% in terms of strength and energy, respectively. The associated reduction in the case of sheets combined with straight strips was even higher, in the order of 80% (strength) and 85% (energy).

When a comparison of the test results is made in terms of *stiffness* (Table 2), most strengthening configurations resulted in higher stiffness values compared with the control joints. These values ranged from about 5% to 40% in the early cycles ($\delta = 5$ mm), from 20% to 90% at $\delta = 25$ mm, and from nearly 0% to 100% at the end of the displacement history ($\delta = 45$ mm). The highest increases were obtained when FRP sheets were anchored using transverse wrapping (joint F22W). The results for the pre-damaged joint (F22in) demonstrated that after a certain displacement level (about 10 mm in this study) even low FRP area fractions ($\rho_{fb} = \rho_{fc} = 0.0026$ here) result in considerable stiffness increase, which was up to about 50% in this study. Finally, when the comparison is made in terms of the rate of stiffness degradation, the conclusion is that this quantity is not affected much by the configuration of the FRP strengthening system.

Conclusions

The tests performed in this study demonstrated that externally bonded FRP reinforcement is a viable solution towards enhancing the strength, energy dissipation, and stiffness characteristics of poorly detailed (in shear) RC joints subjected to simulated seismic loads. Relatively low FRP area fractions increased both the strength (peak lateral load capacity) and the cumulative dissipated energy up to about 70–80%. The increase in stiffness varied with the imposed displacement level and reached values in the order of 100%.

The design of specimens allowed for an investigation of several variables, details of which are described above. The main conclusions, in terms of strength and energy dissipation may be summarized in a rather simplified and qualitative manner as follows:

- Debonding dominates the behavior of external reinforcement unless very low area fractions are employed or proper mechanical anchorages are provided.
- For the same reinforcement area fraction, flexible sheets are more effective than strips.
- Both the strength and the dissipated energy increase considerably with—but not proportionally (due to premature debonding) to—the number of FRP layers.
- Increasing the FRP area fraction in the beam is nearly as effective as it is for equal increase in both the beam and the column, implying that the effectiveness of column FRP is rather limited.
- Mechanical anchorages increase the effectiveness of both strips and sheets. Wrapping of longitudinal FRP sheets with transverse layers proved to be a highly effective anchorage system.
- The effect of high axial load on the shear capacity of FRP-strengthened joints is quite positive.
- If the strengthened joint is damaged (but not repaired), FRP materials are less effective in terms of energy dissipation as opposed to strength increase (both quantities increase though).
- On the basis of the same axial rigidity, glass fiber sheets proved marginally more effective than carbon fiber sheets. However, this is the result of one test only, and further investigation on this topic is needed.
- The effectiveness of FRP increases as the transverse steel reinforcement in the joint decreases.
- Compared with planar specimens, the effectiveness of FRP sheets in joints with a transverse beam is reduced (not so much for the energy as for the strength).

The authors' view is that future research in the area of FRP-strengthened RC joints should be directed towards providing a fundamental understanding of the response when the important failure mode of rebar pull-out dominates over shear failure.

Notation

The following symbols are used in this paper:

K = stiffness;
P = applied load;
δ = imposed displacement;
ρ_{fb} = area fraction of FRP reinforcement in the beam; and
ρ_{fc} = area fraction of FRP reinforcement in the column.

References

Alcocer, S., and Jirsa, J. O. (1993). ''Strength of reinforced concrete frame connections rehabilitated by jacketing.'' *ACI Struct. J.,* 90(3), 249–261.

Antonopoulos, C. P., and Triantafillou, T. C. (2002). ''Analysis of FRP-strengthened RC beam-column joints.'' *J. Compos. Constr.,* 6(1), 41–51.

Beres, A., El-Borgi, S., White, R. N., and Gergely, P. (1992). "Experimental results of repaired and retrofitted beam-column joint tests in lightly reinforced concrete frame buildings." *Technical Rep. No. NCEER-92-0025*, State Univ. of New York at Buffalo, Buffalo, N.Y.

Castellani, A., Negro, P., Colombo, A., Grandi, A., Ghisalberti, G., and Castellani, M. (1999). "Carbon fiber reinforced polymers (CFRP) for strengthening and repairing under seismic actions." *Special Publication No. I.99.41*, European Laboratory for Structural Assessment, Joint Research Center, Ispra, Italy.

Geng, Z.-J., Chajes, M. J., Chou, T.-W., and Pan, D. Y.-C. (1998). "The retrofitting of reinforced concrete column-to-beam connections." *Compos. Sci. Technol.,* 58, 1297–1305.

Gergely, J., Pantelides, C. P., Nuismer, R. J., and Reaveley, L. D. (1998). "Bridge pier retrofit using fiber-reinforced plastic composites." *J. Compos. Constr.,* 2(4), 165–174.

Gergely, J., Pantelides, C. P., and Reaveley, L. D. (2000). "Shear strengthening of RC T-Joints using CFRP composites." *J. Compos. Constr.,* 4(2), 56–64.

Ghobarah, A., Aziz, T. S., and Biddah, A. (1997). "Rehabilitation of reinforced concrete frame connections using corrugated steel jacketing." *ACI Struct. J.,* 4(3), 283–294.

Mosallam, A. (1999). "Seismic repair and upgrade of structural capacity of reinforced concrete connections: Another opportunity for polymer composites." *Proc., Int. Composites Expo '99*, Cincinnati, 1-8.

Pantelides, C. P., Gergely, I., Reaveley, L. D., and Nuismer, R. J. (1997). "Rehabilitation of cap beam-column joints with carbon fiber jackets." *Proc., 3rd Int. Symposium on Non-Metallic (FRP) Reinforcement for Concrete Structures*, Sapporo, Japan, Japan Concrete Institute, Tokyo, 1, 587–595.

Pantelides, C. P., Gergely, J., Reaveley, L. D., and Volnyy, V. (1999). "Retrofit of RC bridge pier with CFRP advanced composites." *J. Struct. Eng.,* 125(10), 1094–1099.

Paulay, T., and Priestley, M. J. N. (1992). *Seismic design of reinforced concrete and masonry buildings*, Wiley, New York.

Tsonos, A. D., and Stylianidis, K. A. (1999). "Pre-seismic and post-seismic strengthening of reinforced concrete structural subassemblages using composite materials (FRP)." *Proc., 13th Hellenic Concrete Conf.*, Rethymno, Greece, 1, 455–466 (in Greek).